Earth and Planetary Science Letters 307 (2011) 135–146

Contents lists available at ScienceDirect

Earth and Planetary Science Letters

journal homepage: www.elsevier.com/locate/epsl

Thermo-chemical evolution and global contraction of mercury

M. Grott [a,*], D. Breuer [a], M. Laneuville [b]

[a] Institute of Planetary Research, German Aerospace Center (DLR), Rutherfordstraße 2, 12489 Berlin, Germany
[b] Institut de Physique du Globe de Paris, Saint Maur des Fossés, France

ARTICLE INFO

Article history:
Received 11 January 2011
Received in revised form 26 April 2011
Accepted 28 April 2011
Available online 18 May 2011

Editor: Y. Ricard

Keywords:
Mercury
Mercury interior
thermal histories
Geophysics

ABSTRACT

The very limited amount of global contraction observed on Mercury's surface poses severe constraints on models of the planet's thermo-chemical evolution and current models rely on a very refractory, Thorium rich composition to slow planetary cooling. However, a refractory composition appears to be incompatible with evidence for pyroclastic eruptions, which require a substantial amount of volatiles to be present in the planetary interior. Furthermore, volcanic activity appears to have been ongoing for a considerable part of the planet's history, while current models predict an early cessation of crustal production. To address these inconsistencies we have reinvestigated the thermo-chemical evolution of Mercury using a non-refractory compositional model, taking the presence of a thermally insulating regolith layer into account. We find that models with a stiff mantle rheology satisfy the observational constraints if the regolith layer is at least 2 km thick. In these models, inefficient mantle convection and thermal insulation significantly slow planetary cooling and prolong the phase of crustal production to 2.5 Gyr after core formation, allowing the volume increase associated with mantle differentiation to offset some of the radial contraction caused by planetary cooling. Models furthermore predict substantial core sulfur contents above 6 wt.%, average crustal thicknesses between 10 and 40 km, and secular cooling rates of 30 K/Gyr.

1. Introduction

The surface of Mercury exhibits a global system of tectonic landforms called lobate scarps, which bear witness to periods of global planetary contraction. Early estimates of the amount of crustal shortening and radial contraction associated with these features range from 1 to 2 km and an average throw of 1 km along the faults has been estimated (Strom et al., 1975). Using the same dataset, but estimating fault displacement using displacement-length scaling relations, Watters and Nimmo (2010) estimated contractional strain corresponding to a radius decrease of only 0.4 to 0.6 km, but the discovery of previously unrecognized lobate scarps in recently acquired MESSENGER images indicates that the number and total length of thrust faults have been underestimated. Latest estimates for the global decrease in radius have been corrected to 0.6 to 0.8 km (Watters et al., 2009), but due to limits imposed by the lighting conditions, these new estimates must be viewed as lower bounds. Furthermore, uncertainties connected to the value of the displacement-length scaling parameter make these estimates uncertain to a factor of 2 or more (Watters et al., 2000).

Watters et al. (2009) estimated that when global image coverage at near optimum lighting conditions is available from the orbital phase of the MESSENGER mission, and when additional new constraints on shortening from the deformation of small craters are obtained, the decrease in Mercury's radius subsequent to the end of the heavy bombardment inferred from the population of lobate scarps will be in the range of 1 to 2 km, as originally estimated by Strom et al. (1975). However, the possible existence of long-wavelength, low-amplitude folds not visible in imagery or currently available topography could imply a further increase in the total planetary radius change (Dombard et al., 2001), and it should be kept in mind that the actual contraction could be slightly larger.

The extremely limited amount of radial contraction observed on the planetary surface poses severe constraints on the planet's evolution and, in particular, the state of its core. Freezing of a purely iron core would result in a radial contraction of 17 km (Solomon, 1976), but would be even larger if a light alloying element such as sulfur were present. This implies that either core freezing must have occurred very early in Mercury's history, eliminating the evidence of radial contraction during the late heavy bombardment, or that the inner core must be quite small (Schubert et al., 1988).

The presence of a liquid outer core is supported by studies of Mercury's libration, which indicate that Mercury's mantle is mechanically decoupled from its core and that the core is at least partially molten (Margot et al., 2007). In order to keep the core from freezing, models require either a heat source like potassium (Solomon, 1976), or an anti-freeze like sulfur (Hauck et al., 2004; Schubert et al., 1988) to be present in the core, where the latter is usually chosen because of its cosmochemical abundance (Cameron, 1973). Thermal evolution models compatible with the observed small contraction require sulfur

* Corresponding author.
E-mail address: matthias.grott@dlr.de (M. Grott).

0012-821X/$ – see front matter © 2011 Elsevier B.V. All rights reserved.
doi:10.1016/j.epsl.2011.04.040

contents of the order of >7 wt.% (Hauck et al., 2004) to prevent substantial inner core freezing.

Mercury's mean density is extremely large, implying an iron to silicate ratio which is about twice that of other terrestrial planets, and two classes of models trying to account for this anomalously high density exist (see Cameron et al., 1988 for a review). The first class of models assumes that part of the silicate shell was removed after core formation during one or more giant impact events, while the second class of models assumes that fractionation between iron and silicates took place during planetary accretion. The first class of models would result in a bulk abundance of heat producing elements close to their primordial concentrations (Cameron et al., 1988), and there are two sub-classes corresponding to the second scenario: Either, heat producing elements will be present according to their equilibrium condensation concentrations (BVSP, 1981), or the high temperatures in the solar nebula could have led to a late stage evaporation of silicates (Fegley and Cameron, 1987), leaving a very refractory, Thorium rich composition behind.

Secular cooling significantly adds to the planetary contraction and radius changes in excess of 2 km are obtained if average mantle temperatures drop by more than 50 K (Hauck et al., 2004). This limits acceptable compositional models to slowly cooling models with a refractory, Thorium rich composition (Fegley and Cameron, 1987), which appears to be at odds with evidence for pyroclastic eruptions documented in recent MESSENGER images. High magma volatile contents above >0.36 wt.% are required to emplace pyroclasts to the observed distances (Kerber et al., 2009), but refractory models seem to preclude the presence of significant concentrations of volatiles in the planet's interior.

New results from the MESSENGER mission indicate that volcanism on Mercury probably extended well into the second half of solar system history (Prockter et al., 2010), while Mariner 10 images showed no evidence for substantial additions to the crust after the end of the late heavy bombardment (e.g., Spudis and Guest (1988)). Crustal production and mantle differentiation are associated with a net volume increase, which can offset some of the contraction caused by secular cooling and inner core formation. Kirk and Stevenson (1989) proposed that mantle differentiation could be responsible for the low amount of global contraction observed on the Moon, but Hauck et al. (2004) dismissed this possibility for Mercury on the grounds that no evidence for late stage volcanism could be found in Mariner 10 imagery. Models by Hauck et al. (2004) produce most of their crust in the early phases of planetary evolution, and the apparent longevity of volcanism on Mercury remains unexplained in their models.

Here we reinvestigate the coupled thermal and crustal evolution of Mercury taking the presence of a poorly conducting megaregolith layer, a thermally insulating crust, and a compositional model which allows for the presence of volatiles in the planetary interior into account. Thermal insulation reduces the amount of secular cooling and extends the time span in which global magmatism occurs beyond the end of the LHB (Breuer et al., 2007), and we will comprehensively analyze the range of acceptable parameters compatible with the small observed radial contraction and the longstanding volcanic activity in the following.

2. Modeling

2.1. Thermal evolution

Mercury's thermo-chemical evolution and the temperatures in the planetary interior are modeled starting from an initial temperature profile and integrating the energy balance equations for the core, mantle and lithosphere as a function of time. Planetary evolution is driven by the efficiency of mantle energy transport and, being in the stagnant lid mode of mantle convection, planetary cooling primarily proceeds by growth of the stagnant lid while keeping the deep interior relatively warm.

The energy balance in the core is given by

$$\left(\rho_c c_c V_c \epsilon_c - \left(L + E_g\right) A_c \rho_c \frac{\partial R_i}{\partial T_c}\right) \frac{dT_c}{dt} = -q_c A_c \tag{1}$$

where ρ_c and c_c are the density and heat capacity of the core, V_c is the core volume, T_c is the temperature at the core–mantle boundary, and ϵ_c is the ratio between the average and core–mantle boundary temperatures. A_c is the surface area of the core, q_c is the heat flux out of the core into the mantle and t is time. The second term on the left hand side of Eq. (1) accounts for the release of latent heat L and gravitational potential energy E_g upon freezing of an inner core, and R_i is the inner core radius. The change of the inner core radius as a function of core–mantle boundary temperature is calculated by comparing the Fe–FeS melting curve to the core adiabat and we adopt the approach by Sevenson et al. (1983), but use updated melting relations for the Fe–FeS system (Fei et al., 1997, 2000).

Energy conservation in the mantle is given by

$$\rho_m c_m V_l \epsilon_m (1 + St)\ \frac{dT_m}{dt} = -\left(q_l + (\rho_{cr} L_{cr} + \rho_{cr} c_{cr} (T_m - T_l)) \frac{dD_{cr}}{dt}\right) A_l + q_c A_c + Q_m V_l \tag{2}$$

where ρ_m and c_m are the density and heat capacity of the mantle, V_l is the volume of the convecting mantle, A_l is the corresponding surface area, and St is the Stefan number which accounts for the consumption and release of latent heat during melting and crystallization of mantle rock. T_m is the upper mantle temperature, ϵ_m is the ratio between the average and upper mantle temperature, and q_l is the heat flux from the convecting mantle into the base of the stagnant lid. D_{cr} is the crustal thickness and the term proportional to the crustal growth rate dD_{cr}/dt accounts for additional heat lost from the convecting mantle due to volcanic heat piping. ρ_{cr} and c_{cr} are the crustal density and heat capacity, respectively, L_{cr} is the latent heat of melting, and T_l is the temperature at the base of the stagnant lid. The mantle volumetric heating rate Q_m depends on the amount and distribution of heat producing elements in the interior and different formation scenarios leading to different choices of Q_m will be discussed in Section 2.3.

Mantle melting and crust formation are calculated by comparing mantle temperatures to the solidus and liquidus of peridotite and while melt is assumed to be extracted instantaneously, melt is produced at the speed scale of mantle convection (Schubert and Spohn, 1990; Spohn, 1991). This is due to the fact that convection is the rate limiting mechanism for providing fresh undepleted material to the global melt channel. Mantle energy transport is determined using scaling laws for stagnant lid convection (Reese et al., 1998; Solomatov and Moresi, 1997) and we use the parameterization by Grasset and Parmentier (1998) and boundary layer theory (Turcotte and Schubert, 2002) to determine q_c and q_l from a Nu–Ra scaling relationship. The model is similar to that applied by Hauck et al. (2004) and details of the applied melting model and scaling laws are given in Morschhauser et al. (2011).

The growth of the stagnant lid is determined by the energy balance at the lithospheric base (Schubert et al., 1979; Schubert and Spohn, 1990; Spohn, 1991; Spohn and Schubert, 1982), which is given by

$$\rho_m c_m (T_m - T_l) \frac{dD_l}{dt} = -q_l + (\rho_{cr} L_{cr} + \rho_{cr} c_{cr} (T_m - T_l)) \frac{dD_{cr}}{dt} - k_m \left.\frac{\partial T}{\partial r}\right|_{r=R_l} \tag{3}$$

where D_l is the stagnant lid thickness, k_m is the mantle thermal conductivity and $\partial T/\partial r|_{r=R_l}$ is the thermal gradient at the base of the stagnant lid.

The removal of heat from the lithospheric base is determined by the thermal gradient at $r=R_l$, which is calculated by solving the heat conduction equation in the lid

$$\frac{1}{r^2}\frac{\partial}{\partial r}\left(r^2 k_l \frac{\partial T}{\partial r}\right) + Q_l = 0. \tag{4}$$

Here, r is the radial distance from the planetary center and k_l and Q_l are the thermal conductivity and heat production rate in the stagnant lid, respectively. These have to be replaced by their respective values k_m, k_{cr}, and k_{reg} and Q_m, Q_{cr}, Q_{reg} in the lithospheric mantle, crust, and regolith layer. As the regolith layer is chemically identical to the crust, we will assume $Q_{cr}=Q_{reg}$ in the following. In principle, Q_{reg} would need to be reduced according to the porosity of the megaregolith, but given that porosity is expected to be ~20% (Warren and Rasmussen, 1987) and that the regolith layer is very thin, this effect is expected to be negligible. As boundary conditions, the surface temperature T_s and the temperature T_l at the base of the stagnant lid are used. By including a heat-piping term proportional to the crustal growth rate in Eq. (3) we assume that the bulk of the extracted melt originates from a region close to or inside the upper thermal boundary layer. This assumption is justified by the small Rayleigh numbers and associated large thermal boundary layer thicknesses usually encountered in Mercury's interior.

Solving Eq. (1)–(3) yields the core–mantle boundary temperature $T_c(t)$, the upper mantle temperature $T_m(t)$, as well as the thicknesses of the upper and lower thermal boundary layers $\delta_u(t)$ and $\delta_c(t)$ as a function of time. The temperature profile in the stagnant lid $T(r,t)_l$ is known from Eq. (4) and given the above quantities, it is straightforward to construct the whole planet temperature profile $T(r,t)$ by assuming temperature to increase linearly in the thermal boundary layers and adiabatically in the mantle and core.

2.2. Planetary contraction

Given the temperature profile in the interior as a function of time, the change of the planetary radius is calculated from the volume changes associated with thermal expansion and contraction of the mantle and core, volume changes connected to partial mantle melting and differentiation, and volume changes connected to the growth of an inner core. To calculate the radius changes associated with secular cooling we consider the volume change due to thermal expansion and contraction ΔV_{th} as a function of time t. Integrating the definition of the thermal expansion coefficient ΔV_{th} is given by

$$\frac{\partial \Delta V_{th}}{\partial t} = \int_{V_p} \alpha(r)\frac{\partial T(r,t)}{\partial t} dV \tag{5}$$

where $\alpha(r)$ is the material dependent coefficient of thermal expansion and the volume integral extends over the entire planetary volume V_p. Due to the adiabatic temperature profile in the core, the core temperature change is only a function of the change of the core–mantle boundary temperature and the integral can be solved analytically between 0 and R_c. Furthermore, integrating Eq. (5) with respect to time, the planetary radius change corresponding to ΔV_{th} is given by

$$\Delta R_{th} = \alpha_c\left(T_c - T_{c,0}\right)\frac{R_c^3}{3R_p^2} + \frac{1}{R_p^2}\int_{R_c}^{R_p} \alpha_m\left(T(r)-T_0(r)\right)r^2 dr \tag{6}$$

where α_c and α_m are the coefficients of thermal expansion for the core and mantle, respectively, $T_{c,0}$ is the initial core–mantle boundary temperature, and $T_0(r)$ is the initial temperature profile in the silicate part of the planet.

The change of planetary radius associated with mantle differentiation and the extraction of partial melt from the mantle are parameterized in terms of the volume fraction of extractable crustal components f and the volume change upon differentiation $\delta V/V$. The change of the total silicate volume ΔV_{md} is then given by

$$\frac{\partial \Delta V_{md}}{\partial t} = \frac{1}{f}\frac{\delta V}{V}\frac{\partial V_{cr}}{\partial t} \tag{7}$$

where V_{cr} is the volume of the crust. Integrating this expression with respect to time and assuming that radius changes are small when compared to the planetary radius, this volume change is equivalent to a change of the planetary radius by

$$\Delta R_{md} = \frac{1}{f}\frac{\delta V}{V}\left(D_{cr} - D_{cr,0}\right) \tag{8}$$

where $D_{cr,0}$ is the thickness of the primordial crust.

Inner core freezing results in the formation of a pure iron inner core, from which light alloying elements are excluded. These elements consequently accumulate in the liquid outer core and the volume change upon core solidification ΔV_{ic} can be parameterized by the density difference between the density ρ_s of pure solid iron and the density ρ_l of the liquid FeS phase. It is given by

$$\frac{\partial \Delta V_{ic}}{\partial t} = \frac{\rho_l - \rho_s}{\rho_l}\frac{\partial V_i}{\partial t} \tag{9}$$

where V_i is the volume of the inner core. The densities of the solid inner and liquid outer core ρ_l and ρ_s are calculated using a third order Birch–Murnaghan equation of state given by

$$p = \frac{3K_0}{2}\left[\left(\frac{\rho}{\rho_0}\right)^{\frac{7}{3}} - \left(\frac{\rho}{\rho_0}\right)^{\frac{5}{3}}\right]\left[1 + \frac{3}{4}\left(K_0' - 4\right)\left(\left(\frac{\rho}{\rho_0}\right)^{\frac{2}{3}} - 1\right)\right] \tag{10}$$

where p is pressure, ρ is density, ρ_0 is the density at reference pressure and temperature, and K_0 and K_0' are the isothermal bulk modulus and its first derivative with respect to pressure, respectively. Density differences across the outer and inner core are neglected and outer core density is calculated using a pressure p corresponding to the core–mantle boundary in Eq. (10), whereas inner core density is determined at a pressure appropriate for the inner core–outer core boundary. While the former is taken to be constant, the latter is a function of the inner core radius.

The densities of pure γ-Fe ρ_{Fe} and FeS ρ_{FeS} are then calculated using the appropriate values for ρ_0, K_0 and K_0' in Eq. (10) and we use the parameters given by Riner et al. (2008) for γ-Fe and those provided by Urakawa et al. (2004) for FeS. The density of the mixed Fe–FeS system is then given by

$$\rho_{Fe-FeS} = \left(\frac{1-\chi_{FeS}}{\rho_{Fe}} + \frac{\chi_{FeS}}{\rho_{FeS}}\right)^{-1} \tag{11}$$

where $\chi_{FeS}=\chi_S(1+M_{Fe}/M_S)$ is the sulfur content in the liquid and M_{Fe} and M_S refer to the molar masses of iron and sulfur, respectively. Following Van Hoolst and Jacobs (2003), the density of liquid Fe–FeS is finally given by $\rho_l = 0.965\rho_{Fe-FeS}$. The density of the pure-iron solid inner core is given by $\rho_s=\rho_{Fe}$.

Integrating Eq. (9) with respect to time, the volume change associated with inner core freezing corresponds to a change of the planetary radius by

$$\Delta R_{ic} = \frac{\rho_l - \rho_s}{\rho_l}\frac{R_i^3}{3R_p^2} \tag{12}$$

if $\Delta R_{ic} \ll R_p$.

The total change of the planetary radius is finally given by the sum of the different components, i.e.,

$$\Delta R_p = \Delta R_{th} + \Delta R_{md} + \Delta R_{ic} \tag{13}$$

where the contributions by mantle differentiation and inner core solidification always result in extension and contraction, respectively, while the sign of ΔR_{th} depends on the specific model. While the thermal evolution will in general lead to planetary cooling, early phases of moderate mantle heating can be encountered for large mantle viscosities.

To compare the amount of calculated planetary contraction to the crustal shortening observed on Mercury's surface (Watters et al., 2009), we assume that the lithosphere can be treated as an elastic shell overlying an effectively fluid layer, in which stresses will be relaxed by subsolidus creep (Hauck et al., 2004; Kirk and Stevenson, 1989; Turcotte, 1983). In this case, the tangential surface strain ε_t is connected to a change of the planetary radius ΔR_p by

$$\varepsilon_t\left(R_p\right) = \frac{\Delta R_p}{R_p} \tag{14}$$

and the corresponding tangential surface stress is given by

$$\sigma_t\left(R_p\right) = \frac{E}{1-\nu}\frac{\Delta R_p}{R_p} \tag{15}$$

where E is Young's modulus and ν is the Poisson ratio (Turcotte, 1983). In this model, all volume changes associated with processes in the interior will result in tangential surface stresses, which will eventually be released in the form of brittle deformation of the elastic shell. This deformation can then be compared to the observed surface strain.

The simple formulation adopted here differs from the approach chosen by Hauck et al. (2004), who explicitly take the presence of an elastic shell into account and include thermo-elastic stresses in the calculation of lithospheric stresses as a function of radius. Although thermo-elastic stresses in a cooling lithosphere add an extensional stress component at depth (Turcotte, 1983), surface stresses remain unaffected due to the prescribed constant surface temperature. Therefore, lithospheric thermo-elastic stresses can be neglected for the purpose of this study. Furthermore, due to the similar compressibility of lithospheric shell and viscous interior, the restraining effect of the elastic shell on extension and contraction is expected to be negligible (Kirk and Stevenson, 1989), such that the results presented here can be directly compared to those obtained by Hauck et al. (2004).

2.3. Parameters

The model parameters most affecting the total contraction obtained in the thermo-chemical evolution calculations are the initial upper mantle temperature T_{m0}, the rheology of the mantle, the abundance of radiogenic elements in the planetary interior, as well as the volume change $\delta V/V$ associated with mantle differentiation. Additionally, the crustal conductivity structure, i.e., the thickness and thermal conductivity of the brecciated regolith layer as well as the conductivity of the intact crustal rock, have a large influence on the obtained contraction. These parameters are summarized in Table 1 and will be discussed in the following in some detail, whereas other parameters used in the calculations are summarized in Table 2.

Table 1
Parameters varied in this study.

Variable	Physical meaning	Value	Units
R_c	Core radius	1840 and 2050	km
T_{m0}	Initial upper mantle temperature	1650–2000	K
ΔT_{cm}	Core excess temperature	0–300	K
k_{cr}	Crustal thermal conductivity	1.5–4	W m^{-1} K^{-1}
η_{ref}	Reference viscosity	10^{19}–10^{22}	Pa s
D_{Reg}	Regolith thickness	$0–5\times10^3$	m
$\delta V/V$	Volume change upon mantle differentiation	0–5	%

Table 2
Fixed parameters used in this study.

Variable	Physical meaning	Value	Units
R_p	Planetary radius	2440	km
g	Surface gravity	3.7	m s^{-2}
T_s	Surface temperature	440	K
ρ_{cr}	Crustal density	2800	kg m^{-3}
ρ_m	Mantle density	3400	kg m^{-3}
ρ_d	Depleted mantle density	3450	kg m^{-3}
ρ_c	Core density	7200	kg m^{-3}
c_{cr}	Magma heat capacity	1000	J kg^{-1} K^{-1}
c_m	Mantle heat capacity	1212	J kg^{-1} K^{-1}
c_c	Core heat capacity	465	J kg^{-1} K^{-1}
ϵ_m	Ratio of mean and upper mantle temperature	1.0	
ϵ_c	Ratio of mean and upper core temperature	1.1	
R	Gas constant	8.3144	J K^{-1} mol^{-1}
T_{ref}	Reference temperature	1600	K
A	Activation energy	3×10^5	J mol^{-1}
k_{Reg}	Regolith thermal conductivity	0.2	W m^{-1} K^{-1}
k_m	Mantle thermal conductivity	4	W m^{-1} K^{-1}
κ	Mantle thermal diffusivity	10^{-6}	m^2 s^{-1}
α_m	Mantle thermal expansion coefficient	2×10^{-5}	K^{-1}
α_c	Core thermal expansion coefficient	3×10^{-5}	K^{-1}
Ra_{crit}	Critical Rayleigh number	450	
Λ	Crustal enrichment factor	4	
L_{cr}	Latent heat of melting	6×10^{-5}	J kg^{-1}
L_+E_g	Energy release during core solidification	2.5×10^{-5}	J kg^{-1}
E_g	Gravitational energy release	2.5×10^{-5}	J kg^{-1}
u_0	Convection speed scale	2×10^{-12}	m s^{-1}
$D_{l,0}$	Initial stagnant lid thickness	50	km
$D_{cr,0}$	Primordial crustal thickness	5	km
f	Fraction of extractable crust	0.4	

Initial upper mantle temperatures after core formation are poorly constrained but warm accretion scenarios appear to be more likely (Schubert et al., 1988). In order to allow for a rapid core formation, initial mantle temperatures should be close to the solidus and significant gravitational energy would have been released during the core formation process. Therefore, T_{m0} should be 1650–2200 K, consistent with the range of initial temperatures investigated by Hauck et al. (2004). However, we will find later that temperatures in excess of 1900 K will result in too large contractional contributions due to secular cooling and limit our analysis in Section 3.4 to temperatures below 2000 K.

Lacking samples from Mercury, the planet's mantle mineralogy is largely unconstrained and we need to investigate a wide range of possible mantle viscosities. Depending on the mantle water content typical reference viscosities η_{ref} of 10^{19} to 10^{22} Pa s are expected at a reference temperature of 1600 K if the rheology is dominated by deformation of olivine (Karato and Wu, 1993; Mackwell, 1991; Mei and Kohlstedt, 2000a,b), see also the review by (Karato, 2010). In addition, it has been suggested that Mercury's mantle might contain larger fractions of pyroxenes (Schubert et al., 1988), which deform less easily than olivine (Bystricky and Mackwell, 2001; Dimanov et al., 2003), and reference viscosities for a pyroxene rich composition are expected to vary between 10^{20} and 10^{22} Pa s for wet and dry pyroxenes, respectively (Chen et al., 2006). However, given that deformation is governed by the weakest mineral, a substantial amount of pyroxenes would need to be present in order to control the viscosity. Given the range of viscosities discussed above, we will vary η_{ref} between 10^{19} and 10^{22} Pa s, spanning the entire plausible range stretching from a wet olivine to a dry pyroxene/olivine rheology.

Estimates of Mercury's bulk composition depend on the adopted formation scenario and different models compatible with the planet's large average density have been proposed. As refractory models appear to be ruled out by the presence of pyroclastic deposits on Mercury's surface (Kerber et al., 2009), models assuming a late stage evaporation of silicates (Fegley and Cameron, 1987) will not be considered here. Alternative scenarios encompass equilibrium condensation models (BVSP, 1981) and the possibility that one or more giant impacts stripped

part of Mercury's mantle, leaving an essentially chondritic composition behind (Cameron et al., 1988). Furthermore, meteoritic mixing models assume that planets and chondrites underwent identical fractionation processes and derive Mercury's bulk composition by mixing four different meteoritic components (Morgan and Anders, 1980).

Potassium is one of the elements found in Mercury's exosphere (Leblanc and Doressoundiram, 2011; Potter and Morgan, 1986, 1997) and we give preference to the model by Morgan and Anders (1980), which allows for some amount of potassium to be present. The present day concentrations of heat producing elements in this model are 34 ppb U, 122 ppb Th, and 69 ppm K, respectively. Note, however, that for the purpose of this study the choice of the compositional model is of secondary importance, as long as the adopted model allows some volatiles to be present in the planetary interior. With respect to the enrichment of radioactive elements in the crust we assume a crustal enrichment factor of 4 with respect to the undepleted mantle, typical for enrichments found at Mid Ocean Ridge Basalts (BVSP, 1981).

Laboratory measurement of the thermal conductivity of volcanic and plutonic rocks range from 0.5 to 4.5 W m^{-1} K^{-1} at ambient conditions (Clauser and Huenges, 1995) and porosity is the controlling factor for volcanic rock thermal conductivity.

Considering that we will treat the high porosity regolith separately in this study and that the majority of volcanic and plutonic rocks have thermal conductivities between 1.5 and 3.5 W m^{-1} K^{-1}, we will vary k_{cr} between 1.5 and 4 W m^{-1} K^{-1}, where the latter value is typical for the thermal conductivity of mantle rock (Hofmeister, 1999).

Similar to the Moon, Mercury's surface is heavily cratered and the near surface layers have been successively reworked by impact gardening. Warren and Rasmussen (1987) have estimated the thickness of the lunar regolith to be 2–3 km and although Mercury's gravity is more than a factor of two larger than that of the Moon and pores are expected to close at shallower depth, the velocity of impactors is expected to be higher for the same reason. Therefore, the thickness of the regolith layer on Mercury can be expected to be of the same order as that on the Moon and we will vary D_{Reg} between 0 and 5 km. Regolith thermal conductivity k_{Reg} has been estimated from the correlation of conductivity with porosity and Warren and Rasmussen (1987) estimate k_{Reg} to be 0.2 W m^{-1} K^{-1}, which is the value adopted here.

The volume change $\delta V/V$ associated with mantle differentiation as well as the fraction f of extractable crustal components from the undepleted mantle depend on the unknown mantle mineralogy and composition of the crustal rocks. Given the amount of extractable crust f as a fraction of the mantle volume, the mantle density ρ_m, the crustal density ρ_{cr}, and the density of the depleted mantle after extraction of the crustal components ρ_d, the volume change upon mantle differentiation may be expressed as

$$\frac{\delta V}{V} = f(1-\gamma) + \frac{\rho_m - f\rho_{cr}}{\rho_d} - 1 \tag{16}$$

where γ is the ratio of extrusive to intrusive volcanism. Although γ is currently unconstrained on Mercury there is evidence for intrusive activity (Denevi et al., 2009; Head et al., 2008, 2009) and the ratio of extrusive to intrusive volcanism is usually small on the terrestrial planets (e.g., Lillis et al., 2009; White et al., 2006). γ ranges from 1/5 to 1/17 for intracontinental volcanism on the Earth (White et al., 2006) and using $\rho_m = 3500$ kg m^{-3}, $\rho_d = 3450$ kg m^{-3}, $\rho_{cr} = 2800$ kg m^{-3}, and $f = 0.4$, we obtain $1 < \delta V/V < 6.5$ % for this range of γ. Being slightly more conservative, we vary $\delta V/V$ between 0 and 5%. Note that $\delta V/V$ primarily depends on ρ_{cr} and larger crustal densities result in smaller expansion. Therefore, if the density of Mercury's crust is similar to that of lunar basalts and $\rho_{cr} \sim 3300$ kg m^{-3} (e.g., Kirk and Stevenson, 1989), $-3 < \delta V/V < 2$%. In this case, the net volume effect of mantle differentiation may indeed be negative if $\gamma > 1/8$.

Mercury's mantle is a relatively thin silicate shell and larger core radii result in noticeably reduced mantle Rayleigh numbers. Therefore, in addition to the parameters discussed above, core size has some influence on the efficiency of mantle energy transport and a self-consistent treatment of core sulfur content χ_S versus R_c should in principle be implemented (e.g., Harder and Schubert, 2001; Riner et al., 2008). However, large uncertainties are associated with models of Mercury's interior structure and we therefore choose to investigate two end-member core radii here. In general, we will assume a core radius of 1840 km, which is compatible with core sulfur contents between 0 and 8% (Riner et al., 2008), and the influence of a larger core radius of 2050 km will be discussed in Section 4.

3. Results

3.1. Influence of thermal insulation

We start off by studying the influence of an insulating layer on the thermal evolution and global contraction by calculating some representative models including a thermally insulating layer, which we then compare to models without such a layer. To better study the influence of insulation on global contraction it is instructive to ignore core freezing for the present discussion, and all models considered in this section have core sulfur contents χ_s large enough to prevent inner core freeze-out. Furthermore, we concentrate on models in the center of the admissible parameter range and choose a reference model with an initial upper mantle temperature T_{m0} of 1750 K, a core excess temperature ΔT_{cm} of 200 K, and a reference viscosity of 10^{21} Pa s.

Results of the calculations are summarized in Fig. 1, and we start the discussion by disregarding radius changes associated with mantle differentiation and choosing $\delta V/V = 0$. For these models, the total planetary radius change ΔR_p is shown as a function of time in Fig. 1a and models do not possess an insulating crust or regolith layer. The total amount of planetary contraction since core formation then is close to 9 km for $T_{m0} = 1750$ K, but changes by ± 3 km if the initial upper mantle temperature is increased or decreased by 100 K. If only contraction after the end of the late heavy bombardment around 4 Gyr b.p. is considered, these values change to 7, 8, and 8 km for $T_{m0} = 1650$, 1750 and 1850 K, respectively, and are still well exceeding the limit posed by fault observations. These results are in agreement with those obtained by Hauck et al. (2004), who found that models using bulk radiogenic abundances corresponding to a condensation type model cool too fast to be compatible with the observed small contraction.

If a thermally insulating crust with conductivity $k_{cr} = 2$ W m^{-1} K^{-1} and a regolith layer with $D_{reg} = 3$ km, $k_{reg} = 0.2$ W m^{-1} K^{-1} are included in the model, planetary cooling and global contraction are significantly reduced. Results of these calculations are shown in Fig. 1b, where the total amount of planetary contraction is reduced to 6 km for $T_{m0} = 1750$ K and changes by $+2$ and -2 km for $T_{m0} = 1850$ and 1650 K, respectively. Considering contraction since the end of the late heavy bombardment, these values are reduced to 4, 5 and 6 km for $T_{m0} = 1650$, 1750, and 1850 K, respectively.

However, a global insulation layer will not only inhibit planetary contraction by slowing secular cooling, but also keep the mantle temperatures above solidus for an extended period of time. In models including a low conductivity crust and regolith layer, the global melt channel typically persists up to 2.5 Gyr after core formation, well beyond the end of the late heavy bombardment, and volume changes associated with mantle differentiation can offset some of the contraction caused by secular cooling. Models without a globally insulating layer cool much faster and produce crust only within the first few hundred Myr (Hauck et al., 2004), such that this mechanism has previously not been considered.

Results of the calculations for $T_{m0} = 1750$ K and $\delta V/V = 1$, 3 and 5% are shown in Fig. 1c as a function of time. A phase of global expansion caused by mantle differentiation occurs during the early evolution and offsets the contribution from secular cooling. Only after 1.5 Gyr does secular cooling outweigh the contribution from the waning crust

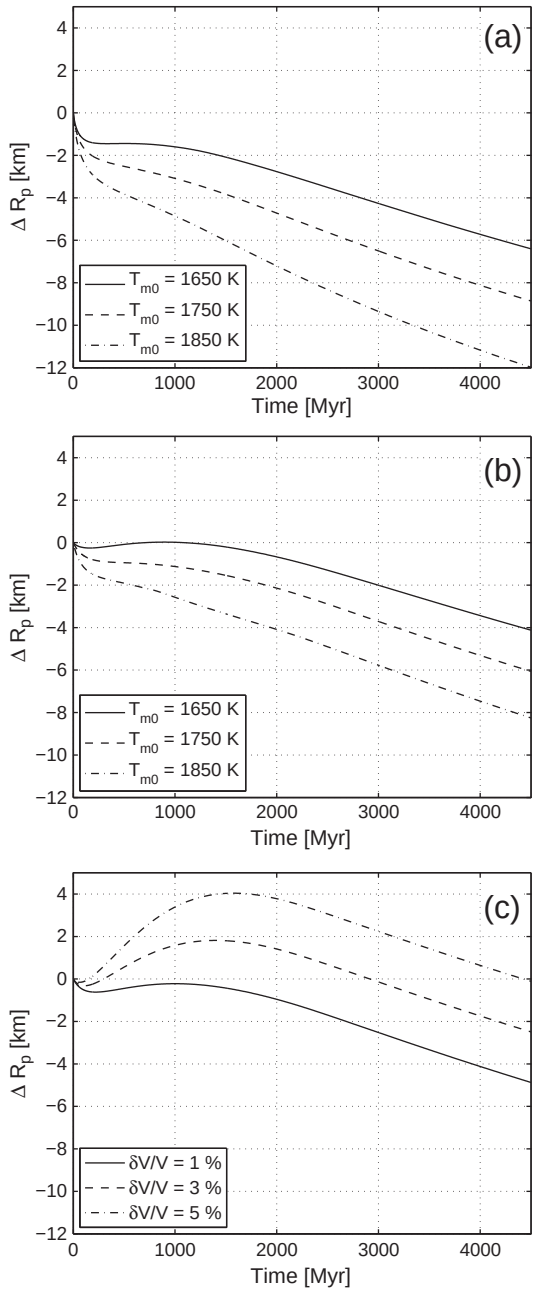

Fig. 1. (a) Total radius change ΔR_p as a function of time t for three different initial upper mantle temperatures T_{m0}. No thermally isolating crust or regolith layer is included, i.e., $k_c = 4$ W m^{-1} K^{-1} and $D_{reg} = 0$ km. The reference viscosity η_0 is 10^{21} Pa s. (b) Same as (a), but including a thermally isolating crust and regolith layer, i.e., $k_c = 2$ W m^{-1} K^{-1} and $D_{reg} = 3$ km. (c) Same as (b), but for an initial upper mantle temperature of 1750 K and varying the volume change upon mantle differentiation $\delta V/V$.

production and the total present day global contraction is 5, 2.5 and 0 km for $\delta V/V = 1$, 3, and 5%, respectively. Measured from the end of the late heavy bombardment, the total contraction is 4, 3, and 2 km for these models, moving them into the range of contractions compatible with the observations.

The phases of global expansion observed in these models might appear to be problematic, as extensional tectonic features on Mercury are not globally distributed (Watters et al., 2009). Rather, the few examples of extensional tectonism observed on Mercury's surface are associated with the Caloris and Raditladi impact basins (Strom et al., 2008), and their origin is attributed to local processes. However, in order to produce visible surface features, the extensional stresses associated with a net volume increase need to exceed the threshold posed by the bounding stress for frictional sliding, and this will in general not be exceeded by a limited amount of global expansion.

The bounding stress for frictional sliding σ_B may be estimated by $\sigma_B > 0.78\sigma_v$ (Mueller and Phillips, 1995), where $\sigma_v = \rho_{cr} g Z$ is the overburden pressure and g and Z are the surface gravitational acceleration and lithospheric thickness, respectively. Assuming the lithosphere to act as a thin elastic shell surrounding an effectively fluid region (Kirk and Stevenson, 1989), the tangential stress in the lithosphere σ_t is given by Eq. (15). Assuming tangential and bounding stresses to be equal, and adopting values of $E = 100$ GPa and $\nu = 0.25$, a radius change of 1 km will generate stresses large enough to induce extensional sliding to a depth of only 5 km. Typical values for the lithospheric thickness at the end of the late heavy bombardment are expected to be of the order of 35 km (Watters et al., 2002), and a volume increase resulting in radius changes of only ~1 km is therefore not expected to induce lithosphere scale faulting.

3.2. Influence of core freezing

Up to now, we have ignored radius changes caused by the freezing of an inner core and we will turn to this problem in the present section. Freezing of an inner core is connected to a substantial decrease of the total core volume and the total radius change associated with freezing of the entire core has been estimated to be 17 km on the basis of a purely iron core (Solomon, 1976). However, this effect can be considerably amplified if a light alloying element such as sulfur is present in the core. Light elements will be expelled from the inner core upon solidification, increasing the density difference between the liquid and solid core phases.

We have calculated the total planetary radius change as a function of inner core size for different core bulk sulfur contents and the results of the calculations are shown in Fig. 2a. Already small inner core sizes of $R_i/R_c = 0.2$ result in global contraction of 1 km. For $R_i/R_c = 0.4$, the associated global contraction already significantly exceeds the amount of contraction observed on the surface, posing severe constraints on the admissible inner core sizes.

In the following we will assume that only a small inner core has solidified, such that the contribution from inner core freeze-out can to first order be neglected in the radius balance. We will then a-posteriori calculate the sulfur content $\chi_{S,min}$ necessary to prevent inner core solidification, which depends on the temperature T_{cm} at the core mantle boundary. Fig. 2b shows $\chi_{S,min}$ as a function of T_{cm} and for core mantle boundary temperatures between 1800 and 1900 K typically encountered in our simulations, $\chi_{S,min}$ is between 6 and 8 wt.%. Note that in order to be compatible with a core dynamo driven by compositional convection (Christensen, 2006; Schubert et al., 1988; Takahashi and Matsushima, 2006; Vilim et al., 2010), the actual sulfur content in Mercury's core needs to be slightly smaller than the minimum value, thus allowing for a small inner core to form at the present day.

3.3. Representative thermo-chemical evolution model

A representative thermo-chemical evolution model including the effects of a thermally insulating crust and inner core freeze-out is shown in Fig. 3. Model parameters are an initial upper mantle temperature T_{m0} of 1700, an initially super-heated core with $\Delta T_{cm} = 200$ K, a crustal thermal conductivity k_{cr} of 2 W m^{-1} K^{-1}, a low conductivity regolith layer of thickness $D_{reg} = 4$ km, a reference viscosity η_0 of $= 10^{21}$ Pa s, and a volume change of mantle differentiation of $\delta V/V = 0.04$. The core sulfur content of the model is chosen to be $\chi_S = 8$ wt.%, allowing for the formation of an inner core toward the end of the evolution.

Fig. 3a shows the upper mantle temperature T_m as well as the temperature at the core–mantle boundary T_{cm} as a function of time. At the beginning of the evolution, the core is superheated with respect to the mantle and T_{cm} exceeds T_m by 280 K. During the early evolution,

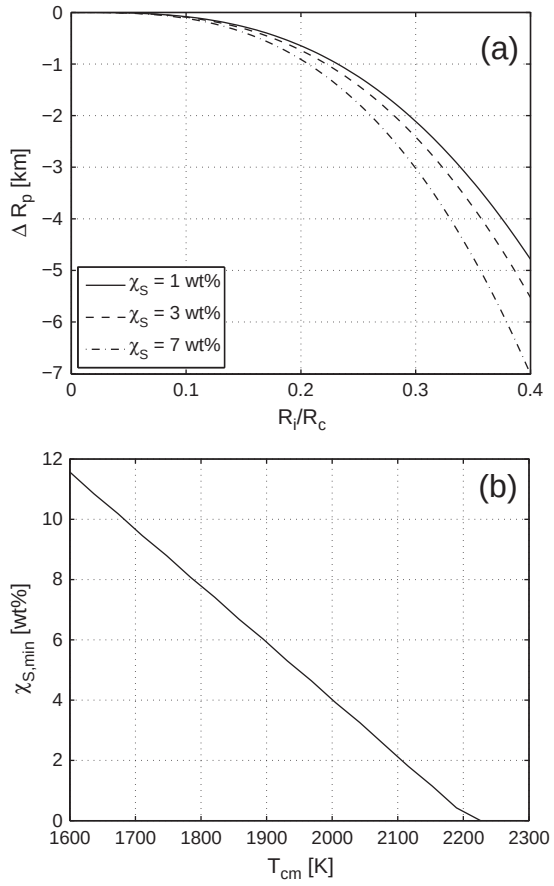

Fig. 2. (a) Total radius change ΔR_p as a function of inner core size R_i normalized to the core radius R_c for different initial core sulfur contents χ_S. (b) Minimum admissible core sulfur content before the start of freezing of an inner core for different core–mantel boundary temperatures T_{cm}.

the mantle heats up as heat is lost from the core and the high mantle viscosity inhibits efficient convective energy transport. At around 500 Myr, the temperature difference between upper mantle and core–mantle boundary is reduced to 70 K, corresponding to the adiabatic temperature increase across the mantle. This difference remains quasi constant throughout the rest of the evolution, until a present day upper mantle temperature of 1700 K and a core–mantle temperature of 1780 K are reached. Note that upper mantle and core temperatures are not entirely representative for the bulk planetary cooling, as the planet primarily looses heat by growth of the stagnant lid. Therefore, although the present day T_m is larger than the initial upper mantle temperature T_{m0}, a net radius contraction is still associated with the planet's thermal evolution.

The heat flows from the core into the mantle q_c, from the mantle into the stagnant lid q_m, as well as the surface heat flow q_s are shown in Fig. 3b as a function of time. The surface heat flow quickly reaches values around 25 mW m^{-2}, and slowly declines to a present day value of 15 mW m^{-2} as radioactive heat sources in the mantle decay. These values are consistent with surface heat flux estimates derived from tectonic modeling, which derive heat flows in the range of 10–43 mW m^{-2} at 4 Gyr b.p. (Watters et al., 2002). Mantle heat flow starts off at 10 mW m^{-2} and slightly increases as the mantle heats up and mantle convection becomes more efficient. Once the mantle starts to cool, q_m decreases and reaches values of 9 mW m^{-2} today. Core heat flows are large as long as the core is still superheated with respect to the mantle, but drop to zero after 400 Myr. T_{cm} then stays constant until after 1 Gyr, when core cooling again proceeds and today's core heat flows reach values around 3.5 mW m^{-2}.

Fig. 3c shows the evolution of the crustal thickness D_c (dashed line), the stagnant lid thickness D_l (solid line), and the extent of the global melt layer (shaded gray) as a function of time. The model starts off with a primordial crustal thickness of 5 km, and D_{cr} steadily grows within the first 2.5 Gyr to values of 42 km. At this point in time the global melt channel vanishes, but further volcanic activity could be connected to decompression melting in the heads of mantle plumes, a process not modeled here. The stagnant lid thickness quickly grows to values around 130 km, indicating fast planetary cooling during the early evolution. Today's values of the stagnant lid thickness are around 225 km, indicating the presence of a massive lid and associated large elastic thicknesses.

Fig. 3c shows the different contributions ΔR from secular cooling, mantle differentiation, and the growth of an inner core to the planetary radius change ΔR_p. Furthermore, the total planetary radius change is also given. Planetary cooling accounts for more than 4 km of planetary contraction, but this decrease of the planetary volume is partially offset by the volume increase associated with mantle differentiation, which results in a moderate planetary extension which peaks around 2 km at 1.6 Gyr. The remaining evolution is governed by planetary cooling, until an inner core starts to solidify at around 4.2 Gyr. Inner core growth adds more than 1 km of planetary contraction within only 300 Myr, increasing the total amount of contraction to slightly more than 3 km. Measured from the end of the late heavy bombardment, net extension is reduced to <1.5 km, while the total contraction is increased to 3.5 km.

The model presented in Fig. 3 is a typical example for models showing little planetary contraction while assuming a composition which allows for the presence of volatiles. First of all, low contraction models show large mantle viscosities and/or low initial upper mantle temperatures, leading to a phase of early mantle heating and episodes of low or negative core heat flows. Second, the presence of a thermally insulating layer helps to maintain the temperatures in the mantle above solidus for an extended period of time, allowing for the production of crust up to times late in the evolution. Finally, a phase of moderate extension associated with mantle differentiation is observed in most models. Although global systems of extensional tectonic features are not observed on Mercury (Watters et al., 2009), small amounts of contraction around 1 km are not expected to produce visible surface faults (see Section 3.1). A more systematic investigation of the parameter space and a classification of the admissible model parameters will be presented in the following section.

3.4. Admissible models

To investigate the range of models compatible with the observations, we define an admissible model by the following criteria: 1) The total amount of global extension after the end of the late heavy bombardment shall not exceed 1 km. 2) The total amount of global contraction after the end of the late heavy bombardment shall not exceed 3 km. 3) The present day crustal thickness shall be larger than 10 km. Note that we have slightly increased the admissible amount of global contraction with respect to the values estimated by Watters et al. (2009). In this way we take into account that present estimates must be regarded as lower limits, and we will treat models satisfying the tighter constraint of $\Delta R_p > -2$ km separately in the following discussion.

Using the above criteria, we investigated the parameter space spanned by $1600 < T_{m0} < 1900$ K, $10^{19} < \eta_{ref} < 10^{22}$ Pa s, $0 < \Delta T_{cm} < 300$ K, $0 < \delta V/V < 5\%$, $1.5 < k_{cr} < 4$ W m^{-1} K^{-1}, and $0 < D_{reg} < 5$ km. We picked 10,000 random combinations of these parameters and determined admissible models by comparing the results of the individual model run with the criteria given above. Out of the 10,000 models, only 273 were found to be admissible. Furthermore, only 17 models showed global contraction smaller than 2 km.

The results of the computations are given in Fig. 4, where all admissible models are shown as green dots, while models satisfying

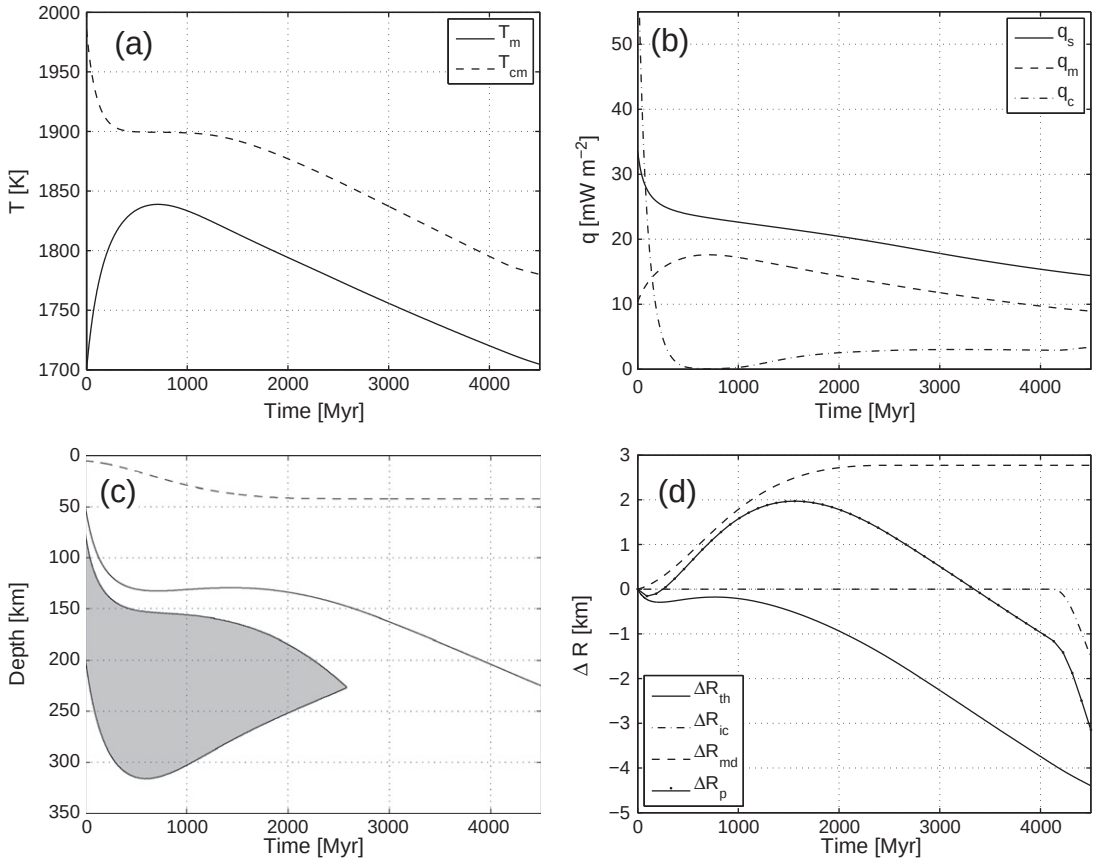

Fig. 3. Representative thermal evolution model for Mercury having $T_{m0}=1700$ K, $\Delta T_{cm}=200$ K, $k_{cr}=2$ W m^{-1} K^{-1}, $D_{reg}=4$ km, $\eta_0=10^{21}$ Pa s, $\delta V/V=0.04$, and $\chi_S=8$ wt.%. (a) Upper mantle temperature T_m and the temperature at the core–mantle boundary T_{cm} as a function of time. (b) Surface heat flux q_s, mantle heat flux q_m, and core heat flux q_c as a function of time. (c) Evolution of the crustal thickness D_c (dashed line), the stagnant lid thickness D_l (solid line), and the extent of the global melt layer (shaded gray) as a function of time. (d) Different contributions ΔR to the global planetary radius change ΔR_p as a function of time.

the tighter constraint of $\Delta R_p > -2$ km are shown in red. Fig. 4a shows a scatter plot of the admissible models as a function of reference viscosity η_{ref} and initial upper mantle temperature T_{m0}, i.e., those combinations of η_{ref} and T_{m0} for which a set of ΔT_{cm}, $\delta V/V$, k_{cr}, and D_{reg} was found such that 1)–3) are satisfied. Successful models require small amounts of secular cooling and either have low initial upper mantle temperatures or large mantle viscosities (or both). While essentially all initial upper mantle temperatures are admissible, reference viscosities below 10^{20} Pa s were found not to be compatible with the observations.

Fig. 4b shows successful models as a function of crustal thermal conductivity k_{cr} and regolith thickness D_{reg}. We find that the regolith layer thickness needs to exceed a thickness of 2 km in order to comply with the observational constraints, and only if $D_{reg}>4$ km $\Delta R_p > -2$ km is obtained. Models without a thermally insulating layer result in too large contractions, consistent with the results by Hauck et al. (2004) and the results presented in Section 3.1.

Present day crustal thicknesses of the admissible models are presented as a function of initial upper mantle temperature in Fig. 4c, with most models showing crustal thicknesses between 10 and 40 km. Only few models have $D_{cr}>40$ km and models with $\Delta R_p > -2$ km fall within the range $10<D_{cr}<50$ km. There is a tendency for models with larger initial upper mantle temperatures to yield larger present day crustal thicknesses, as would be expected for a warmer planetary interior.

The minimum bulk sulfur content $\chi_{s,min}$ necessary to prevent core freezing is given in Fig. 4d as a function of initial upper mantle temperature T_{m0}. $\chi_{s,min}$ needs to exceed 6 wt.% in all models and models with low initial upper mantle temperatures may require as much as 10 wt.% of sulfur to be compatible with the observed low planetary contraction. A general trend is visible and while the range of minimum sulfur contents is large for small T_{m0}, $\chi_{s,min}$ need not exceed 6–7% for $T_{m0}>1750$ K.

To be compatible with a core dynamo driven by compositional convection (Christensen, 2006; Schubert et al., 1988; Takahashi and Matsushima, 2006; Vilim et al., 2010), the actual sulfur content in Mercury's core needs to be slightly smaller than the minimum value required to prevent the initiation of inner core freeze-out. Therefore, the sulfur contents given in Fig. 4d should be interpreted accordingly. However, given the uncertainties associated with the knowledge of the core adiabat and the Fe–S melting relations, $\chi_{s,min}$ can serve as a valuable estimate for the actual sulfur content compatible with only a small amount of planetary contraction contributed by the growth of an inner core.

The amount of secular cooling after 500 Myr encountered in successful models is shown as a function of initial upper mantle temperature in Fig. 4e. For most models, secular cooling after the end of the late heavy bombardment is below 120 K, but can be as large as 160 K for larger initial upper mantle temperatures. The temperature evolution of the admissible models is shown as a function of time in Fig. 4f, where it is evident that all models follow a similar trend. Mantle temperatures increase by up to 200 K during the earliest evolution, before secular cooling dominates after 500 to 1000 Myr. Secular cooling is relatively slow and the cooling rate is close to 30 K/Gyr in most models, slightly smaller than that reported for Mars by Morschhauser et al. (2011), but well below the average cooling rate of

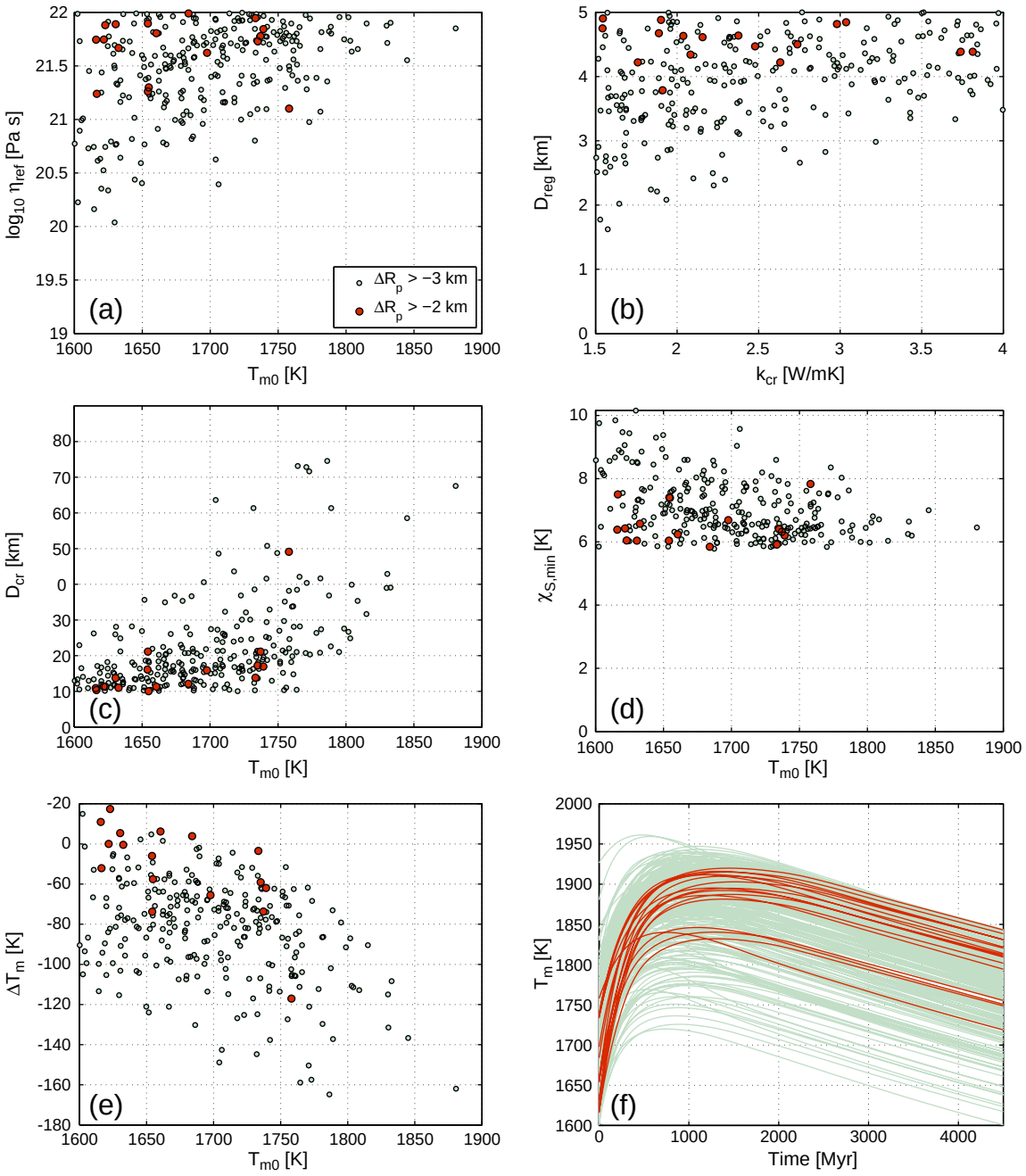

Fig. 4. (a) Scatter plot of successful models which show less than 1 km of global expansion and 3 km of global contraction since the end of the late heavy bombardment around 4 Gyr b.p. as a function of initial upper mantle temperature T_{m0} and reference viscosity η_{ref}. In addition, models showing less than 2 km of global radial contraction are shown in red. (b) Same as (a), but as a function of regolith thickness D_{reg} and crustal thermal conductivity k_{cr}. (c) Present day crustal thickness D_{cr} as a function of initial upper mantle temperature for successful models. (d) Minimum core sulfur content $\chi_{S,min}$ as a function of initial upper mantle temperature for successful models. (e) Change of the upper mantle temperature ΔT_m after 500 Myr as a function of T_{m0} for successful models. (f) Upper mantle temperature T_m as a function of time for successful models.

the Earth, which is estimated to have been 50 to 100 K/Gyr during the last 3 Gyr (Korenaga, 2008).

For the presented analysis we have assumed a primordial crustal thickness of 5 km, and larger values would result in an early removal of heat producing elements from the interior and reduced subsequent volcanic activity. However, the results presented here remain essentially unchanged if $D_{cr,0} = 20$ km is assumed and 15 out of the 1000 models we tested were found to show admissible global contraction smaller than 3 km, while still showing volcanic activity resulting in present day crustal thicknesses between 20 and 40 km.

4. Conclusions

We have reinvestigated the thermo-chemical evolution of Mercury considering models which are compatible with the presence of volatiles in the planetary interior and taking the presence of a thermally insulating crust and regolith layer into account. We find that Mercury's evolution is significantly influenced by such a layer and that planetary cooling is considerably reduced, extending the period in which a global melt layer exists up to 3 Gyr after core formation. In this way, the volume increase associated with mantle differentiation

can act to compensate some of the contraction associated with planetary cooling and models satisfy the constraints posed by the small overall contraction of the planet, which is estimated to be only 1–2 km (Watters et al., 2009).

Admissible models have low initial upper mantle temperatures between 1600 and 1900 K, a stiff mantle rheology with reference viscosities above 10^{20} Pa s, and possess a poorly conducting megaregolith layer which has to be at least 2 km thick. Core sulfur contents compatible with only a small inner core range from 6 to 10%, and the obtained average crustal thickness is between 10 and 50 km for most models. It should be noted, however, that the minimum amount of sulfur necessary to prevent core freezing determined here depends on the applied Fe–FeS melting relation, and this number might change slightly if a different melting relation were to be used (e.g., Rivoldini et al., 2009).

Model results suggest that the evolution of the magnetic field can be characterized by two periods of dynamo action, with a short-lived thermally driven dynamo operating during the first few hundred million years after core formation (cp. Fig. 3b). During this time period, core heat flow exceeded that conducted along the core adiabat, i.e., about 11 to 15 mW m^{-2} (Hauck et al., 2004; Schubert et al., 1988), thus driving thermal convection in the fluid core. A second period of dynamo action was then triggered by the solidification of a small inner core ($R_i/R_c<0.2$) within the last few hundred million years (compare Fig. 3d), and compositional convection in the fluid outer core with non-eutectic composition could generate the present-day dynamo (Braginsky, 1964).

Various dynamo models consistent with the observed weak magnetic field of Mercury (Anderson et al., 2008; Ness et al., 1974) have been suggested in recent years, but thin-shell models (e.g., Stanley et al. (2005)) require large inner core sizes and $R_i/R_c>0.8$, which is difficult to reconcile with small amounts of global contraction. A model consistent with $R_i/R_c<0.2$ is the deep dynamo model by Christensen (2006) and Christensen and Wicht (2008), which requires a small inner core with $R_i/R_c<0.55$. However, in this model a weak magnetic field is only obtained if the core sulfur concentration is below one percent (Manglik et al., 2010), which likely results in early core freezing and large amounts of planetary contraction.

Recent experimental work on the melting behavior of the iron–sulfur system indicates that Mercury's core might be in a different crystallization regime than what is typically expected for the terrestrial planets (Chen et al., 2008). Experiments imply that precipitation of iron in Mercury's core is not restricted to the inner core–outer core boundary, but can occur at different radii throughout the outer core, depending on sulfur content. Assuming different precipitation zones to be present, (Vilim et al., 2010) carried out numerical dynamo simulations and found that the presence of a so called double snow state, consisting of precipitation zones at the core–mantle boundary and at intermediate depth in the outer core, will provide a source of compositional buoyancy capable of driving a dynamo which is weak enough to be compatible with Mercury's observed magnetic field (Anderson et al., 2009). Double snow zones will be present for core sulfur contents between 8 and 10 wt.%, consistent with the models presented here. Note, however, that the inner core radius of $R_i/R_c=0.34$ chosen by Vilim et al. (2010) is not strictly compatible with the observed small amount of global contraction, as $R_i/R_c=0.34$ would imply $\Delta R_{ic}\approx -4$ km.

An interesting possibility concerning the composition of Mercury's core has recently been suggested by Fei et al. (2011), who argue that Mercury could have accreted under even more reduced conditions than the Earth, and that silicon could be the dominant light element in Mercury's core. Because Si partitions almost equally between solid and liquid FeSi (Kuwayama and Hirose, 2004), the density change and associated contraction upon core solidification would then be expected to be small, allowing for a wider range of possible inner core sizes than determined here. However, in this case compositional buoyancy would not act as a driving force for outer core convection (Fei et al., 2011) and a mechanism other than chemical convection would be required to drive the core dynamo. Alternatively, a minor amount of sulfur could be present in addition to silicon, but this possibility remains to be investigated.

The range of crustal thicknesses obtained in this study is lower than estimates of the local crustal thickness at the Caloris impact basin, which Watters et al. (2005) estimate to be 90 to 140 km. However, their estimate is reduced to 45–70 km if a crustal thermal conductivity of 2 W m^{-1} K^{-1} is assumed, and it is further reduced if a low conductivity regolith layer is taken into account. Therefore, considering that the estimate reflects the local crustal thickness at the Caloris impact basin, average crustal thicknesses calculated here are not incompatible with the results of Watters et al. (2005). Other estimates of crustal thicknesses imply that D_{cr} needs to be smaller than 140 km to fulfill the requirement that the base of the crust does not melt (Nimmo and Watters, 2004), which is consistent with the results obtained here.

The mantle viscosity of admissible models needs to be larger than 10^{20} Pa s and only models with $\eta_{ref}>10^{21}$ Pa s fulfill the stricter requirement of $\Delta R_p>-2$ km. In terms of the mantle mineralogy, these viscosities can be interpreted in a number of different ways, with $\eta_{ref}=10^{21}$ Pa s corresponding to a dry olivine or intermediately wet pyroxene rheology. Likely candidates for the volatile species which could drive pyroclastic eruptions include CO, CO_2, H_2O, and SO_2, such that the presence of substantial amounts of water in the mantle does not seem to be required. Furthermore, even if water is the eruption driving volatile, it could be added to the magma at shallow depth, leaving the deeper mantle essentially dry. Therefore, the relatively large required viscosities are reasonable and can correspond to different plausible mantle mineralogies.

There has been some debate on whether mantle convection exists on Mercury today (Hauck et al., 2004; Redmond and King, 2007), and the physical state of Mercury's mantle depends on the initial Rayleigh number, the amount of heat produced by the decay of radioactive elements, and the heat flow across the core–mantle boundary (Redmond and King, 2007). While Hauck et al. (2004) report the cessation of mantle convection in some of their models, a sluggish mantle convection persists in the two dimensional models favored by Redmond and King (2007), and mantle convection persists to the present day in the three-dimensional simulations by King (2008). In agreement with the results by Redmond and King (2007) and King (2008), all models presented in Section 3 convect to the present day and today's thickness of the actively convecting layer is between 100 and 350 km. This can be attributed to the presence of a thermally insulating layer, resulting in slower planetary cooling. Thus, excessive growth of the thermal boundary layers is prevented and the point where the actively convecting portion of the mantle vanishes is never reached during the evolution. Note also that Redmond and King (2007) argued on the basis of two dimensional convection simulations that parameterized thermal evolution models can overestimate the cooling of the planet during the earliest evolution, such that the results presented here can be viewed as upper limits on the planetary cooling.

In this study, we have treated the core radius to be constant, whereas in reality R_c depends on the core sulfur content. Core radii compatible with the planet's mass and radius range from 1800 to 2100 km for sulfur contents between 1 and 8 wt.% (Harder and Schubert, 2001; Riner et al., 2008; Rivoldini et al., 2009). To evaluate the influence of a larger core, we have calculated 1500 models assuming $R_c=2050$ km, 119 of which showed global contraction below 3 km. Due to the significantly reduced mantle depth and the associated low Rayleigh numbers, these models do not show active mantle convection at the present day, but are in a conductive mode of heat transport. Therefore, models with $R_c=2050$ km loose heat much less efficiently than models with smaller cores and even models without a thermally insulating crust and regolith layer can satisfy $\Delta R_p>-3$ km. However, due to their low Rayleigh numbers, models with larger cores have thicker thermal boundary layers, pushing meltzones to greater depth and mantle melting is suppressed in these

models. Therefore, models with large cores show reduced crustal production and all admissible models show present day crustal thicknesses of less than 10 km. Furthermore, due to their low mantle temperatures, these models require core sulfur contents in excess of 8 wt.% to prevent inner core freezing.

The timing of crustal production has some influence on the total amount of global contraction, and depends – among other things – on the abundance of heat producing elements in the planetary interior. Increasing the concentration of long-lived radioactive species will result in a prolonged phase of crustal production and possibly even smaller amounts of global contraction than reported here. Considering that we have investigated only a single compositional model in this study, it should be kept in mind that different models satisfying the observational constraints are likely to exist. However, there are limits to the range of admissible compositions and models with high potassium and low uranium and thorium content are unlikely to be compatible with model constraints. In particular, out of the 1500 models we tested using a chondritic composition (Cameron et al., 1988), which has four times less thorium and uranium and eight times more potassium than the model considered here (Morgan and Anders, 1980), none was found to be admissible, making a chondritic composition for Mercury highly unlikely.

Acknowledgments

We wish to thank Scott King and Gabriel Tobie for their comments, which helped to improve this manuscript. This research has been supported by the Helmholtz Association through the research alliance “Planetary Evolution and Life”.

References

Anderson, B.J., Acuña, M.H., Korth, H., Purucker, M.E., Johnson, C.L., Slavin, J.A., Solomon, S.C., McNutt, R.L., 2008. The structure of Mercury's magnetic field from MESSENGER's first flyby. Science 321, 82–85.
Anderson, B.J., et al., 2009. The magnetic field of Mercury. Space Sci. Rev. 152, 307–339.
Basaltic Volcanism Study Project, 1981. Basaltic Volcanism on the Terrestrial Planets. Pergamon Press, New York.
Braginsky, S.I., 1964. Magnetohydrodynamics of the Earth's core. Geomag. Aeron. 4, 698–712.
Breuer, D., Hauck, S.A., Buske, M., Pauer, M., Spohn, T., 2007. Interior evolution of Mercury. Space Sci. Rev. 132 (2–4), 229–260. doi:10.1007/s11214-007-9228-9.
Bystricky, M., Mackwell, S., 2001. Creep of dry clinopyroxene aggregates. J. Geophys. Res. 106 (13), 443–454. doi:10.1029/2001JB000333.
Cameron, A.G.W., 1973. Abundances of the elements in the solar system. Space Sci. Rev. 15, 121–146. doi:10.1007/BF00172440.
Cameron, A.G.W., Fegley Jr., B., Benz, W., Slattery, W.L., 1988. The Strange Density of Mercury: Theoretical Considerations. In: Vilas, F. (Ed.), Mercury. University of Arizona Press, Tuscan, pp. 59–164.
Chen, S., Hiraga, T., Kohlstedt, D.L., 2006. Water weakening of clinopyroxene in the dislocation creep regime. J. Geophys. Res. 111 (B8), B08203. doi:10.1029/2005JB003885.
Chen, B., Li, J., Hauck, S.A., 2008. Non-ideal liquidus curve in the Fe–S system and Mercury's snowing core. Geophys. Res. Lett. L07201. doi:10.1029/2008GL033311.
Christensen, U.R., 2006. A deep dynamo generating Mercury's magnetic field. Nature 105–1058. doi:10.1038/nature05342.
Christensen, U.R., Wicht, J., 2008. Models of magnetic field generation in partly stable planetary cores: applications to Mercury and Saturn. Icarus 196, 16–34.
Clauser, C., Huenges, E., 1995. Thermal conductivity of rocks and minerals. In: Ahrens, T.J. (Ed.), Rock Physics and Phase Relations: A Handbook of Physical Constants: AGU Ref. Shelf, vol. 3. AGU, Washington, D.C, pp. 105–126.
Denevi, B.W., Robinson, M.A., Solomon, S.C., Murchie, S.L., Blewett, D.T., Domingue, D.L., McCoy, T.J., Ernst, C.M., Head, J.W., Watters, T.R., Chabot, N.L., 2009. The evolution of Mercury's crust: a global perspective from MESSENGER. Science 324 (5927), 613–618. doi:10.1126/science.1172226.
Dimanov, A., Lavie, M.P., Dresen, G., Ingrin, J., Jaoul, O., 2003. Creep of polycrystalline anorthite and diopside. J. Geophys. Res. 108B1 (2061). doi:10.1029/2002JB001815.
Dombard, A.J., Hauck, S.A., Solomon, S.C., Phillips, R.J., 2001. Potential for long-wavelength folding on Mercury. Lunar Planet. Sci. XLII abstract 2035.
Fegley, B., Cameron, A.G.W., 1987. A vaporization model for iron/silicate fractionation in the Mercury protoplanet. Earth Planet. Sci. Lett. 82 (3–4), 207–222. doi:10.1016/0012-821X(87)90196-8.
Fei, Y., Bertka, C.M., Finger, L.W., 1997. High-pressure iron sulfur compound, Fe_3S_2, and melting relations in the Fe–FeS system. Science 275, 1621–1623.
Fei, Y., Li, J., Bertka, C.M., Prewitt, C.T., 2000. Structure type and bulk modulus of Fe_3S, a new iron–sulfur compound. Am. Mineral. 85, 1830–1833.
Fei, Y., Hillgren, V.J., Shahar, A., Solomon, S.C., 2011. On the silicon content of Mercury's core and implications for core mineralogy, structure, and density. Lunar Planet. Sci. XXXII abstract 1949.
Grasset, O., Parmentier, E.M., 1998. Thermal convection in a volumetrically heated, infinite Prandtl number fluid with strongly temperature-dependent viscosity: implications for planetary evolution. J. Geophys. Res. 103, 18171–18181.
Harder, H., Schubert, G., 2001. Sulfur in Mercury's core? Icarus 151 (1), 118–122. doi:10.1006/icar.2001.6586.
Hauck, S.A., Dombard, A.J., Phillips, R.J., Solomon, S.C., 2004. Internal and tectonic evolution of Mercury. Earth Planet. Sci. Lett. 222, 713–728.
Head, J.W., Murchie, S.L., Prockter, L.M., Robinson, M.S., Solomon, S.C., Strom, R.G., Chapman, C.R., Watters, T.R., McClintock, W.E., Blewett, D.T., Gillis-Davis, J.J., 2008. Volcanism on Mercury: evidence from the First MESSENGER Flyby. Science 321 (5885), 69–72. doi:10.1126/science.1159256.
Head, J.W., Murchie, S.L., Prockter, L.M., Solomon, S.C., Strom, R.G., Chapman, C.R., Watters, T.R., Blewett, D.T., Gillis-Davis, J.J., Fassett, C.I., Dickson, J.L., Hurwitz, D.M., Ostrach, L.R., 2009. Evidence for intrusive activity on Mercury from the first MESSENGER flyby. Earth Plan. Sci. Lett. 285 (3–4), 251–262. doi:10.1016/j.epsl.2009.03.008.
Hofmeister, A.M., 1999. Mantle values of thermal conductivity and the geotherm from phonon lifetimes. Science 283 (5408), 1699–1706. doi:10.1126/science.283.5408.1699.
Karato, S.-I., 2010. Rheology of the deep upper mantle and the implications for the longevity of the continental roots: a review. Tectonophysics 481, 82–98.
Karato, S.-I., Wu, P., 1993. Rheology of the upper mantle: a synthesis. Science 260, 771–778.
Kerber, L., Head, J.W., Solomon, S.C., Murchie, S.L., Blewett, D.T., Wilson, L., 2009. Explosive volcanic eruptions on Mercury: eruption conditions, magma volatile content, and implications for interior volatile abundances. Earth Plan Sci. Lett. 285, 263–371.
King, S.D., 2008. Pattern of lobate scarps on Mercury's surface reproduced by a model of mantle convection. Nat Geosci. 1, 229–232. doi:10.1038/ngeo152.
Kirk, R.L., Stevenson, D.J., 1989. The competition between thermal contraction and differentiation in the stress history of the Moon. J. Geophys. Res. 94, 12133–12144.
Korenaga, J., 2008. Urey ratio and the structure and evolution of Earth's mantle. Rev. Geophys. 46, RG2007. doi:10.1029/2007RG000241.
Kuwayama, Y., Hirose, K., 2004. Phase relations in the system Fe–FeSi at 21 GPa. Am. Min. 89 (2–3), 273–276.
Leblanc, F., Doressoundiram, A., 2011. Mercury exosphere: II. The sodium/potassium ratio. Icarus 211, 1, 10–20. doi:10.1016/j.icarus.2010.09.004.
Lillis, R.J., Dufek, J., Bleacher, J.E., Manga, M., 2009. Demagnetization of crust by magmatic intrusion near the Arsia Mons volcano: magnetic and thermal implications for the development of the Tharsis province, Mars. J. Volcan. Geoth. Res 185 (1–2), 123–138.
Mackwell, S.J., 1991. High temperature rheology of enstatite: implications for creep in the mantle. Geophys. Res. Lett. 18, 2027–2030.
Manglik, A., Wicht, J., Christensen, U., 2010. A dynamo model with double diffusive convection for Mercury's core. Earth Planet. Sci. Lett. 289, 619–628.
Margot, J.L., Peale, S.J., Jurgens, R.F., Slade, M.A., Holin, I.V., 2007. Large longitude libration of Mercury reveals a molten core. Science 316 (5825), 710–714. doi:10.1126/science.1140514.
Mei, S., Kohlstedt, D.L., 2000a. Influence of water on plastic deformation of olivine aggregates 1. Diffusion creep regime. J. Geophys. Res. 105 (B9), 21457–21470. doi:10.1029/2000JB900179.
Mei, S., Kohlstedt, D.L., 2000b. Influence of water on plastic deformation of olivine aggregates 2. Dislocation creep regime. J. Geophys. Res. 105 (B9), 21471–21482. doi:10.1029/2000JB900180.
Morgan, J.W., Anders, E., 1980. Chemical composition of Earth, Venus, and Mercury. PNAS 77 (12), 6973–6977. doi:10.1073/pnas.77.12.6973.
Morschhauser, A., Grott, M., Breuer, D., 2011. Crustal recycling, mantle dehydration, and the thermal evolution of Mars. Icarus 212, 541–558. doi:10.1016/j.icarus.2010.12.028.
Mueller, S., Phillips, R.J., 1995. On the reliability of lithospheric constraints derived from models of outer-rise flexure. Geophys. J. Int. 123, 887–902.
Ness, N.F., Behannon, K.W., Lepping, K.P., Whang, Y.C., Schatten, K.H., 1974. Magnetic field observations near Mercury: preliminary results from Mariner 10. Science 185, 151–160.
Nimmo, F., Watters, T.R., 2004. Depth of faulting on Mercury: implications for heat flux and crustal and effective elastic thickness. Geophys. Res. Lett. 31 (2), L02701. doi:10.1029/2003GL018847.
Potter, A.E., Morgan, T.H., 1986. Potassium in the atmosphere of Mercury. Icarus 67, 336–340.
Potter, A.E., Morgan, T.H., 1997. Sodium and potassium atmospheres of Mercury. Planet. Space Sci. 45, 95–100.
Prockter, L.M., Ernst, C.M., Denevi, B.W., Chapman, C.R., Head, J.W., Fassett, C.I., Merline, W.J., Solomon, S.C., Watters, T.R., Strom, R.G., Cremonese, G., Marchi, S., Massironi, M., 2010. Evidence for young volcanism on Mercury from the Third MESSENGER Flyby. Science 329 (5992), 668–671. doi:10.1126/science.1188186.
Redmond, H.L., King, S.D., 2007. Does mantle convection currently exist on Mercury? Phys. Earth Plan. Inter. 164 (3–4), 221–231. doi:10.1016/j.pepi.2007.07.004.
Reese, C.C., Solomatov, V.S., Moresi, L.-N., 1998. Heat transport efficiency for stagnant lid convection with dislocation viscosity: application to Mars and Venus. J. Geophys. Res. 103 (E6), 13643–13658. doi:10.1029/98JE01047.
Riner, M.A., Bina, C.R., Robinson, M.S., Desch, S.J., 2008. Internal structure of Mercury: implications of a molten core. J. Geophys. Res. 113, E08013. doi:10.1029/2007JE002993.
Rivoldini, A., Van Hoolst, T., Verhoeven, O., 2009. The interior structure of Mercury and its core sulfur content. Icarus 12–30. doi:10.1016/j.icarus.2008.12.020.
Schubert, G., Spohn, T., 1990. Thermal history of Mars and the sulfur content of its core. J. Geophys. Res. 95, 14095–14104.
Schubert, G., Cassen, P., Young, R.E., 1979. Subsolidus convective cooling histories of terrestrial planets. Icarus 38, 192–211. doi:10.1016/0019-1035(79)90178-7.

Schubert, G., Ross, M.N., Stevenson, D.J., Spohn, T., 1988. Mercury's thermal history and the generation of its magnetic field. In: Vilas, F., Chapman, C.R., Matthews, M.S. (Eds.), Mercury. University of Arizona Press, Tucson, pp. 429–460.

Sevenson, D.J., Spohn, T., Schubert, G., 1983. Magnetism and thermal evolution of the terrestrial planets. Icarus 54, 466–489. doi:10.1016/0019-1035(83)90241-5.

Solomatov, V.S., Moresi, L.N., 1997. Three regimes of mantle convection with non-Newtonian viscosity and stagnant lid convection on the terrestrial planets. Geophys. Res. Lett. 24 (15), 1907–1910. doi:10.1029/97GL01682.

Solomon, S.C., 1976. Some aspects of core formation in Mercury. Icarus 28 (4), 509–521. doi:10.1016/0019-1035(76)90124-X.

Spohn, T., 1991. Mantle differentiation and thermal evolution of Mars, Mercury, and Venus. Icarus 90, 222–236. doi:10.1016/0019-1035(91)90103-Z.

Spohn, T., Schubert, G., 1982. Modes of mantle convection and the removal of heat from the earth's interior. J. Geophys. Res. 87, 4682–4696.

Spudis, P.D., Guest, J.E., 1988. Stratigraphy and geologic history of Mercury. In: Vilas, F., et al. (Ed.), Mercury. University of Arizona Press, Tuscan, pp. 59–164.

Stanley, S., Bloxham, J., Hutchinson, W.E., Zuber, M.T., 2005. Thin shell dynamo models consistent with Mercury's weak surface magnetic field. Earth Planet. Sci. Lett. 234, 27–38.

Strom, R.G., Trask, N.J., Guest, J.E., 1975. Tectonism and volcanism on Mercury. J. Geophys. Res. 80, 2478–2507.

Strom, R.G., Chapman, C.R., Merline, W.J., Solomon, S.C., Head, J.W., 2008. Mercury cratering record viewed from MESSENGER's first flyby. Science 321, 79–81.

Takahashi, F., Matsushima, M., 2006. Dipolar and non-dipolar dynamos in a thin shell geometry with implications for the magnetic field of Mercury. Geophys. Res. Lett. L10202. doi:10.1029/2006GL025792.

Turcotte, D.L., 1983. Thermal stresses in planetary elastic lithospheres. J. Geophys. Res. 88 (S2), A585–A587. doi:10.1029/JB088iS02p0A585.

Turcotte, D.L., Schubert, G., 2002. Geodynamics, 2nd ed. Cambridge Univ. Press, New York. 456 pp.

Urakawa, S., Someya, K., Terasaki, H., Katsura, T., Yokoshi, S., Funakoshi, K., Utsumi, W., Katayama, W., Sueda, Y., Irifune, T., 2004. Phase relationships and equations of state for FeS at high pressures and temperatures and implications for the internal structure of Mars. Phys. Earth Plan. Int. 143–144, 469–479. doi:10.1016/j.pepi.2003.12.015.

Van Hoolst, T., Jacobs, C., 2003. Mercury's tides and interior structure. J. Geophys. Res. 108, 5121. doi:10.1029/2003JE002126.

Vilim, R., Stanley, S., Hauck, S.A., 2010. Iron snow zones as a mechanism for generating Mercury's weak observed magnetic field. J. Geophys. Res. 115, E11003. doi:10.1029/2009JE003528.

Warren, P.H., Rasmussen, K.L., 1987. Megaregolith insulation, internal temperatures, and bulk uranium content of the moon. J. Geophys. Res. 92, 3453–3465. doi:10.1029/JB092iB05p03453.

Watters, T.R., Nimmo, F., 2010. The tectonics of Mercury. In: Watters, T.R., Schultz, R.A. (Eds.), Planetary Tectonics. Cambridge Univ. Press, Cambridge, UK, pp. 15–79.

Watters, T.R., Schultz, R.A., Robinson, M.S., 2000. Displacement-length relations of thrust faults associated with lobate scarps on Mercury and Mars: comparison with terrestrial faults. Geophys. Res. Lett. 27, 3659–3662.

Watters, T.R., Schultz, R.A., Robinson, M.S., Cook, A.C., 2002. The mechanical and thermal structure of Mercury's early lithosphere. Geophys. Res. Lett. 29 (11), 1542. doi:10.1029/2001GL014308.

Watters, T.R., Nimmo, F., Robinson, M.S., 2005. Extensional troughs in the Caloris Basin of Mercury: evidence of lateral crustal flow. Geology 33, 669–672 2005.

Watters, T.R., Solomon, S.C., Robinson, M.S., Head, J.W., Andr, S.L., Hauck, S.A., Murchie, S.L., 2009. Earth Plan. Sci. Lett. 285, 283–329.

White, S.M., Crisp, J.A., Spera, F.J., 2006. Long-term volumetric eruption rates and magma budgets. Geochem. Geophys. Geosyst. 7, Q03010.